Science and Technology of Advanced Materials

ISSN: (Print) (Online) Journal homepage: www.tandfonline.com/journals/tsta20

High-throughput evaluation of half-metallicity of Co_2MnSi Heusler alloys using composition-spread films and spin-integrated hard X-ray photoelectron spectroscopy

Ryo Toyama, Shunsuke Tsuda, Yuma Iwasaki, Thang Dinh Phan, Susumu Yamamoto, Hiroyuki Yamane, Koichiro Yaji & Yuya Sakuraba

To cite this article: Ryo Toyama, Shunsuke Tsuda, Yuma Iwasaki, Thang Dinh Phan, Susumu Yamamoto, Hiroyuki Yamane, Koichiro Yaji & Yuya Sakuraba (2025) High-throughput evaluation of half-metallicity of Co_2MnSi Heusler alloys using composition-spread films and spin-integrated hard X-ray photoelectron spectroscopy, Science and Technology of Advanced Materials, 26:1, 2439781, DOI: 10.1080/14686996.2024.2439781

To link to this article: https://doi.org/10.1080/14686996.2024.2439781

Published online: 07 Jan 2025.

SCIENCE AND TECHNOLOGY OF ADVANCED MATERIALS
2025, VOL. 26, NO. 1, 2439781
https://doi.org/10.1080/14686996.2024.2439781

Taylor & Francis
Taylor & Francis Group

High-throughput evaluation of half-metallicity of Co_2MnSi Heusler alloys using composition-spread films and spin-integrated hard X-ray photoelectron spectroscopy

Ryo Toyama [a], Shunsuke Tsuda [b], Yuma Iwasaki [c], Thang Dinh Phan [b], Susumu Yamamoto [d,e], Hiroyuki Yamane [f,g], Koichiro Yaji [b,h] and Yuya Sakuraba [a]

[a]Magnetic Functional Device Group, Research Center for Magnetic and Spintronic Materials (CMSM), National Institute for Materials Science (NIMS), Tsukuba, Japan;
[b] Photoemission Spectroscopy Group, Center for Basic Research on Materials (CBRM), National Institute for Materials Science (NIMS), Tsukuba, Ibaraki, Japan;
[c]Data-driven Materials Design Group, Center for Basic Research on Materials (CBRM), National Institute for Materials Science (NIMS), Tsukuba, Japan;
[d]International Center for Synchrotron Radiation Innovation Smart (SRIS), Tohoku University, Sendai, Japan;
[e]Institute of Multidisciplinary Research for Advanced Materials (IMRAM), Tohoku University, Sendai, Japan;
[f]Photon Science Innovation Center (PhoSIC), NanoTerasu, Aramaki-aza-Aoba, Sendai, Japan;
[g]RIKEN SPring-8 Center, RIKEN, Hyogo, Japan;
[h]Unprecedented-scale Data Analytics Center, Tohoku University, Sendai, Japan

ABSTRACT

We demonstrate high-throughput evaluation of the half-metallicity of Co_2MnSi Heusler alloys by spin-integrated hard X-ray photoelectron spectroscopy (HAXPES) of composition-spread films performed with high-brilliance synchrotron radiation at NanoTerasu, which identifies the optimum composition showing the best half-metallicity. $Co_{75-x}Mn_xSi_{25}$ composition-spread thin films for $x = 10$–40% with a thickness of 30 nm are fabricated on MgO(100) substrates using combinatorial sputtering technique. The $L2_1$-ordering and (001)-oriented epitaxial growth of Co_2MnSi are confirmed by X-ray diffraction for $x = 18$–40%. The valence band HAXPES spectra exhibit a systematic compositional dependence and the smallest photoemission intensity at the Fermi level (E_F) for a slightly Mn-rich composition of $x = 27\%$. The density of states (DOS) for $L2_1$-ordered Co_2MnSi with different Mn compositions obtained from first-principles calculation also show the smallest total DOS at E_F for $x = 27\%$ because of the formation of a clear half-metallic gap in the minority spin channel and the less localized *d*-states in the majority spin channel, indicating the best half-metallic nature of this composition. Our experimental results demonstrate that high-throughput evaluation of half-metallicity is possible even with spin-integrated HAXPES by capturing systematic changes in the electronic structures through the measurements on the composition-spread film. Moreover, the anisotropic magnetoresistance (AMR) of the composition-spread film is measured for electric current directions along the [110] and [100] of Co_2MnSi. Previous studies indicated that a larger negative AMR ratio is a signature of a higher spin polarization. The largest negative AMR ratio is observed for $x = 27\%$ for both current directions, which also supports the best half-metallicity for this off-stoichiometric composition.

ARTICLE HISTORY
Received 27 August 2024
Revised 8 November 2024
Accepted 4 December 2024

KEYWORDS
Heusler alloys; half-metallicity; Co_2MnSi; composition-spread films; hard X-ray photoelectron spectroscopy; density of states; anisotropic magnetoresistance effect; NanoTerasu

CONTACT Ryo Toyama TOYAMA.Ryo@nims.go.jp; Yuya Sakuraba SAKURABA.Yuya@nims.go.jp Magnetic Functional Device Group, Research Center for Magnetic and Spintronic Materials (CMSM), National Institute for Materials Science (NIMS), Tsukuba, Ibaraki 305-0047, Japan

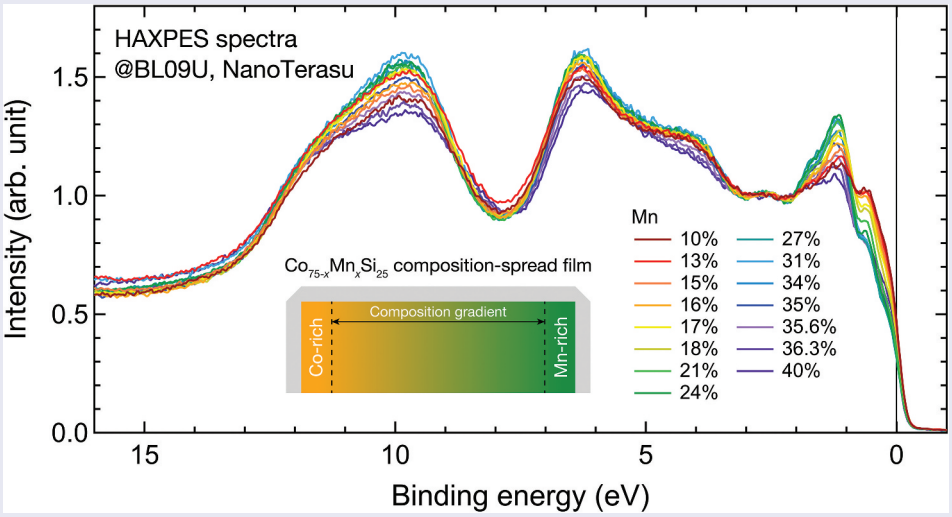

IMPACT STATEMENT

High-throughput systematic measurement of hard X-ray photoelectron spectroscopy for the Co-Mn-Si composition-spread film using the newly developed synchrotron light source NanoTerasu revealed the best composition exhibiting the highest half-metallic nature

1. Introduction

Half-metallic ferromagnets have been considered as promising materials for realizing various efficient spintronics devices [1]. In the electronic band structures of half-metals, one of the spin states has a finite band gap at the Fermi level (E_F), which is called half-metallic gap [1]. Due to the formation of a half-metallic gap, spin polarization (P) that is defined by the difference in the density of states (DOS) between the majority ($D_\uparrow(E_F)$) and minority ($D_\downarrow(E_F)$) spin states at E_F as $P = [D_\uparrow(E_F) - D_\downarrow(E_F)]/[D_\uparrow(E_F) + D_\downarrow(E_F)]$ can be ideally 100% [1]. This leads to a high magnetoresistance ratio in spintronic devices such as current-perpendicular-to-plane giant magnetoresistance (CPP-GMR) [2] and tunnel magnetoresistance (TMR) devices [3,4]. The high spin polarization of half-metallic materials also contributes to an efficient electrical spin injection into semiconductors at room temperature, leading to semiconductor spintronic devices [5,6]. Among the various candidates, Heusler alloys, typically denoted as X_2YZ (*e.g.*, X = Co, Ni; Y = Mn, Fe; Z = Al, Si, Ge, and Ga), are the promising half-metallic materials [7,8]. For example, Co_2MnSi [9–14] has been considered as a robust half-metal that has a large minority gap of up to 0.81 eV [15] and high Curie temperature of 985 K [16]. In fact, the first magnetic tunnel junction (MTJ) device exhibiting a high TMR ratio at room temperature has been demonstrated using the Co_2MnSi as electrodes [3].

The half-metallicity of Heusler alloys strongly depends on the atomic composition (*i.e.*, off-stoichiometry). For example, for Mn-containing Heusler alloys such as Co_2MnSi, Co_{Mn} anti-sites (Co atoms at nominal Mn sites) tend to increase the DOS at E_F in the half-metallic gap, leading to a steep reduction of spin polarization [17–27]. Therefore, careful optimization of the atomic composition of Heusler alloys is inevitable for obtaining half-metallic properties. However, quantitative determination of spin polarization has been difficult because of time-consuming experimental processes for fabricating spintronic devices using lithographic techniques such as nonlocal spin-valve (NLSV) devices [28–31] and CPP-GMR devices [32,33]. Thus, developing a simple, high-throughput evaluation method for half-metallicity is crucial for searching ideal half-metallic Heusler alloys from various candidates including atomic combination and fabrication conditions. Recently, anisotropic magnetoresistance (AMR) measurement has been proposed as a facile evaluation method for half-metallicity of Heusler alloys. It has been demonstrated experimentally that a larger negative AMR ratio corresponds to a higher spin polarization of various Heusler alloys [34–36], which also suggests a smaller DOS at E_F within the half-metallic gap. Thus, the AMR ratio is a good indicator for searching optimized compositions of Heusler alloys. However, although a qualitative correlation between a large negative AMR ratio and high spin polarization has been confirmed, the AMR ratio itself does not give quantitative spin polarization values, which makes AMR measurement an indirect evaluation method for half-metallicity. To increase the throughput of measurements, combinatorial techniques such as using composition-spread films are an effective strategy [37–41]. Although the quantitative determination of spin polarization and compositional optimization

in a Heusler alloy using NLSV devices fabricated from single composition-spread films have been demonstrated [42], it is still time-consuming to fabricate and analyze the NLSV devices for the compositional optimization. The evaluation of spin polarization using CPP-GMR devices would also be time-consuming because the devices with a ferromagnetic layer of various thicknesses have to be prepared using complex lithographic processes [32,33].

Direct observation of electronic structures is the most reliable for evaluating half-metallic electronic structures. This is possible by photoelectron spectroscopy (PES) such as vacuum ultraviolet PES and soft X-ray PES [43–46]. However, these methods are surface-sensitive; the measurements are strongly affected by the surface state due to the short inelastic mean-free path of electrons. In contrast, hard X-ray photoelectron spectroscopy (HAXPES) is a bulk-sensitive probing technique [47–49]. Recently, Ueda *et al.* have reported spin-resolved HAXPES of a 30-nm-thick Co_2MnSi thin film buried under an oxide capping layer to directly evaluate spin-dependent valence band electronic states and confirmed a half-metallic gap and high spin polarization of ≈ 90% [50]. Although spin-resolved HAXPES measurement is a powerful tool for the direct observation of half-metallic gap in the minority spin state [50–53], it is a time-consuming technique; due to the small photoionization cross sections of hard X-rays, HAXPES is inherently an electron-poor measurement, and the efficiency is further reduced by spin resolution. Thus, spin-resolved HAXPES is not an efficient measurement method in principle, which may not be suitable for high-throughput characterization.

Because of the characteristic shape of electronic structures near E_F of the half-metallic Heusler alloys such as Co_2MnSi, *spin-integrated* HAXPES could also detect half-metallic gap formation [54–56], which takes less measurement time compared to that for spin-resolved one. As the calculated DOS will be shown later, in the minority spin state, the low DOS at E_F in the half-metallic gap is surrounded by the two edges of high DOS. The DOS at E_F should be the smallest if there is a half-metallic gap at E_F. On the other hand, in the majority spin state, only a few states contribute to the DOS at E_F emerging from strongly dispersing bands and they would not be largely influenced by the composition. Thus, the total DOS at E_F should be the smallest when the half-metallic gap is formed at E_F and the total DOS at E_F should reflect the existence of half-metallic gap in the minority spin state due to no DOS in the minority spin state and small *sp*-dominated DOS in the majority spin state at E_F. This would lead that if the composition dependence of photoemission intensity near E_F is measured systematically using composition-spread films, it would be possible to evaluate the half-metallicity of Heusler alloys by spin-integrated valence band HAXPES spectra even without time-consuming spin resolution experiments. Therefore, performing spin-integrated HAXPES experiments on Heusler alloy composition-spread films can be a high-throughput method for evaluating half-metallicity. Modak *et al.* have reported spin-integrated HAXPES of $Co_2MnAl_{1-\alpha}Si_\alpha$ composition-spread films performed at BL15XU of SPring-8 [57]. They have successfully observed a systematic shifting of the peak position of the HAXPES spectra toward the higher binding energy, with a total energy shifting of 0.40 eV from the Co_2MnAl to Co_2MnSi side, demonstrating a combinatorial tuning of E_F in the composition-spread film. They have also performed a combinatorial measurement of thermoelectric properties using the composition-spread films. However, the half-metallic gap formation has not been analyzed from the valence band HAXPES spectra at E_F in detail.

In this study, we investigate the Mn-composition dependence on the half-metallicity of Co_2MnSi Heusler alloy using composition-spread films and spin-integrated HAXPES. To overcome a critical issue of inefficiency in the measurement of HAXPES caused by the low photoionization cross sections, we performed the experiment using high-brilliance synchrotron radiation at a newly-built 3 GeV synchrotron light source 'NanoTerasu' in Japan [58–60]. We correlate spin-integrated HAXPES spectra of the composition-spread film with theoretical DOS obtained from first-principles calculation. To verify the half-metallic electronic structures directly observed by HAXPES in terms of transport properties, we also measured the composition dependence of AMR systematically. We show that our experimental results combining composition-spread films and spin-integrated HAXPES demonstrate high-throughput evaluation of the half-metallicity of Co_2MnSi Heusler alloy.

2. Experimental details

2.1. Composition-spread films

$Co_{75-x}Mn_xSi_{25}$ composition-spread thin films with Mn composition x ranging from 10 to 40 at.% were fabricated using a combinatorial sputtering system (CMS-A6250X2, Comet Inc., Japan), as shown in Figure 1(a). Single-crystal MgO(100) substrates with a size of $10 \times 10\ mm^2$ (Furuuchi Chemical Corp., Japan) were cleaned with acetone, ethanol, and deionized water with ultrasonication. The substrates were installed in the deposition chamber and further cleaned by *in situ* Ar-ion milling. First, uniform layers of Co (0.138 nm), Mn (0.047 nm), and Si (0.180 nm) were deposited on the substrates. After that, a wedge-shaped Co layer with a maximum thickness of 0.135 nm was deposited on the uniform Si layer with

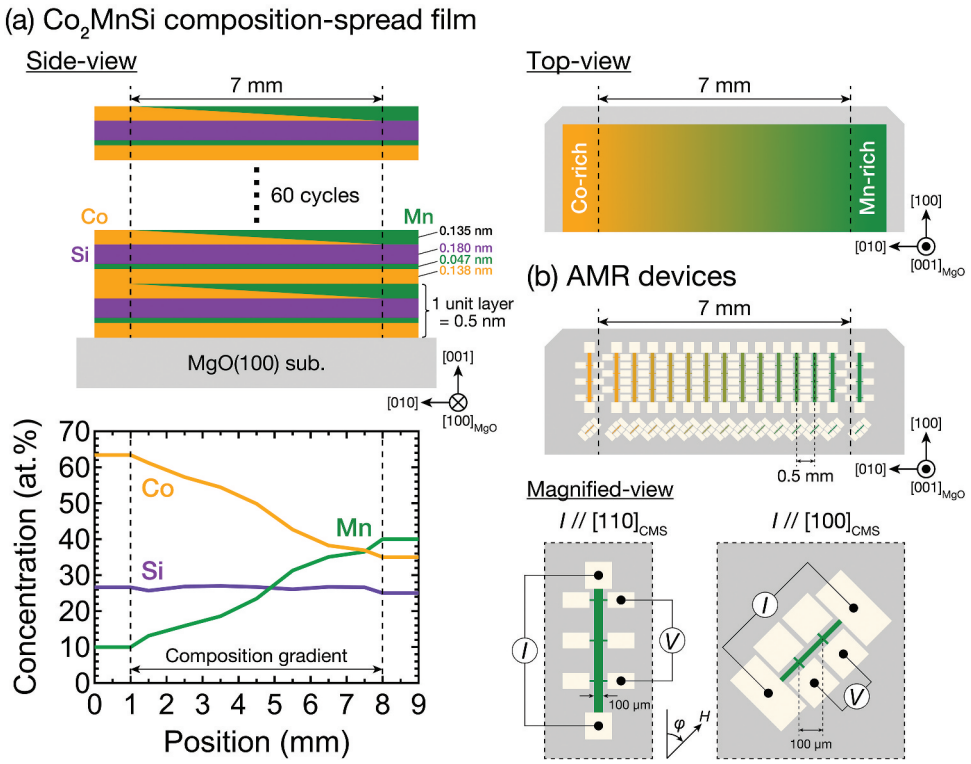

Figure 1. (a) Side-view and top-view schematic diagrams of Co_2MnSi composition-spread thin films ($Co_{75-x}Mn_xSi_{25}$, x = 10–40 at.%) on MgO(100) substrates. The positional dependence of the composition measured by X-ray fluorescence (XRF) is also plotted below the side-view diagram. (b) Top-view schematic diagrams of multiterminal devices for anisotropic magnetoresistance (AMR) measurement. The magnified-views of the AMR devices for the electric current (I) directions along the [110] and [100] of Co_2MnSi (CMS) are also displayed.

a composition gradient width of 7 mm using a linear moving mask. Subsequently, the substrates were rotated by 180°, and a wedge-shaped Mn layer with the same maximum thickness and composition gradient width was deposited on the wedge-shaped Co layer. The deposition process for the one-unit layer of 0.5 nm with a flat surface was repeated 60 times to obtain 30-nm-thick $Co_{75-x}Mn_xSi_{25}$ composition-spread films. The deposition was performed with a substrate temperature of room temperature (RT) and Ar process gas pressure of 0.5 Pa. After the deposition, the films were *in situ* post-annealed at 500°C for 30 min and capped with Al (2 nm) at RT to prevent oxidization.

The positional dependence on the actual composition of the composition-spread films was measured using X-ray fluorescence (XRF; ZSX Primus II, Rigaku, Japan), as plotted in Figure 1(a). For example, compositions for the Co-richest and Mn-richest regions were estimated to be $Co_{63}Mn_{10}Si_{27}$ and $Co_{35}Mn_{40}Si_{25}$, respectively. Thus, the Mn composition was varied from 10% to 40% within the composition-spread film. Hereafter, this composition-spread film is referred to as $Co_{75-x}Mn_xSi_{25}$ with x being the actual composition determined by XRF for simplicity.

The compositional dependence on the crystal structures of the composition-spread films was measured using X-ray diffraction (XRD; SmartLab, Rigaku, Japan) with a collimated Cu-$K\alpha$ radiation by a 0.5 mm incident slit. The measurement position was varied at an interval of 1 mm. It is noted that due to the collimator width of 0.5 mm, each diffraction pattern except for the uniform regions of x = 10% and 40% should include the neighboring composition regions with a maximum of ≈ ±1.8%.

After the XRF and XRD measurements, the film was cut into two pieces; one of them was used for HAXPES experiment and the other for AMR measurement described from the next section. Using the samples from the identical composition-spread film for each measurement enables us to obtain a set of systematic experimental data.

2.2. Hard X-ray photoelectron spectroscopy (HAXPES) experiment

The spin-integrated HAXPES experiment was performed at BL09U of NanoTerasu. The measurement system and vacuum chambers used in the present work were developed at BL15XU of SPring-8 [61] and were transferred to BL09U of NanoTerasu. The composition-spread film was installed in an ultrahigh

vacuum chamber. The synchrotron X-ray with a photon energy of ≈ 6 keV, monochromatized by a symmetrical layout-type double crystal monochromator [62] and a Si(111) channel-cut crystal, was irradiated to the film with a fixed incident angle of 2° relative to the surface parallel. The *p*-polarized X-ray was used to excite photoelectrons, where the electric field oscillates in-plane of the incidence and points to the direction of the electron detector. The irradiation position of X-ray was varied in a vertical direction with an interval of 0.5 mm, which corresponds to the same positions as those of 15 multiterminal devices that will be described later. Using a monolithic Wolter mirror, the incident X-ray beam was focused to 7 × 10 (vertical × horizontal) μm^2, and the footprint of the X-ray beam on the sample at grazing incidence was as small as ≈ 7 × 300 (vertical × horizontal) μm^2. The photoelectrons were detected and analyzed using a high-resolution hemispherical electron analyzer (R4000, Scienta Omicron). The measurement range of kinetic energy was 5932 to 5951 eV with a step of 25 meV, where this energy range refers to the valence band region. The pass energy was set to 100 eV, and the overall energy resolution was ≈ 200 meV. The measurement was performed at room temperature. Owing to the high-brilliance synchrotron radiation, a spectrum with a good signal-to-noise ratio was taken for ≈ 1 h per position. Thus, the HAXPES experiment was completed within only 1 day. The charge-up effect was not observed, and the energy shift of the incident X-ray was carefully calibrated using the peak position of Au $4f_{7/2}$ before and after the measurements of $Co_{75-x}Mn_xSi_{25}$ for each *x*. The binding energy (E_B) was determined using the peak positions of Au $4f_{7/2}$ and E_F of Au.

The obtained raw HAXPES spectra were horizontally shifted considering the energy shift of the incident X-ray for each measurement. Due to this correction of energy offset, data points regarding the energy were different between measurement positions. To match the energy values between the spectra with respect to the $E_B = 0$ eV with a step of 25 meV, the photoemission intensity data were interpolated and complemented.

2.3. Theoretical calculation

The density of states (DOS) of $L2_1$-ordered Co_2MnSi with different Mn compositions were calculated using the AkaiKKR software, which employed the density functional theory (DFT) and the Korringa–Kohn–Rostoker coherent-potential approximation (KKR-CPA) [63–66]. The CPA method can accurately simulate multielemental-disordered phases, especially in alloy systems. The following parameters were set during the calculations; the imaginary part at E_F (*edelt*) was set to 0.001. The parameter *bzqlty*, which impacts the quality of the Brillouin zone mesh, was assigned a value of 10, leading to produce 1062 *k* points. The maximum considered angular momentum (*xml*) was 3. The exchange–correlation potential (*sdftyp*) was set to the local density approximation (*mjw*). The spin-orbit interaction and relativistic effects were considered, thus setting the *reltyp* parameter to *srals*. The width of the energy contour (*ewidth*) was fixed at 1.0. The lattice constant was optimized within the calculation by minimizing the total energy.

2.4. Anisotropic magnetoresistance (AMR) measurement

To evaluate the dependence of composition and electric current direction on the AMR effect, multiterminal devices were fabricated using the remaining composition-spread films by conventional photolithography and Ar-ion milling techniques, as shown in Figure 1(b). The devices were patterned along the [110] and [100] directions of the Co_2MnSi film with 15 devices for each direction, which were aligned to the composition gradient. The device-to-device distance within the composition gradient region was designed to be 0.5 mm. For the [110] devices, the bar width was designed to be 100 μm, which corresponds to the compositional variation with a maximum of ≈ ±0.37% for each bar. For the [100] devices, the horizontal distance between the two terminals was designed to be 100 μm, so that the composition variation for each bar can be the same as that for the [110] devices. The angular-dependent resistivity was measured by a standard DC four-probe method using the Physical Property Measurement System (PPMS Versalab; Quantum Design) with a motorized sample holder. A constant electric current (*I*) of 100 μA was applied to the long-axis of the devices, where the relationship between the directions of *I* and the crystal axis of Co_2MnSi was *I*//[110] and *I*//[100]. A constant external magnetic field (*H*) of 0.3 T, which was enough to saturate the magnetization, was rotated in-plane to the film surface, where the relative angle (φ) was defined from the [110] direction of Co_2MnSi as shown in Figure 1(b). The AMR ratio was defined as $(\rho_{//} - \rho_{\perp})/\rho_{\perp}$, where $\rho_{//}$ ($\rho_{\perp}$) is the resistivity of the films where $\varphi = 0°$ (90°). The measurement was performed at 300 K.

3. Results and discussion

3.1. Crystal structures

The out-of-plane ($\chi = 0°$) and tilted-plane ($\chi = 54.7°$) one-dimensional (1D) XRD patterns of the $Co_{75-x}Mn_xSi_{25}$ composition-spread film are shown in Figure 2(a, b), respectively. Two-dimensional (2D) XRD images for $\chi =$

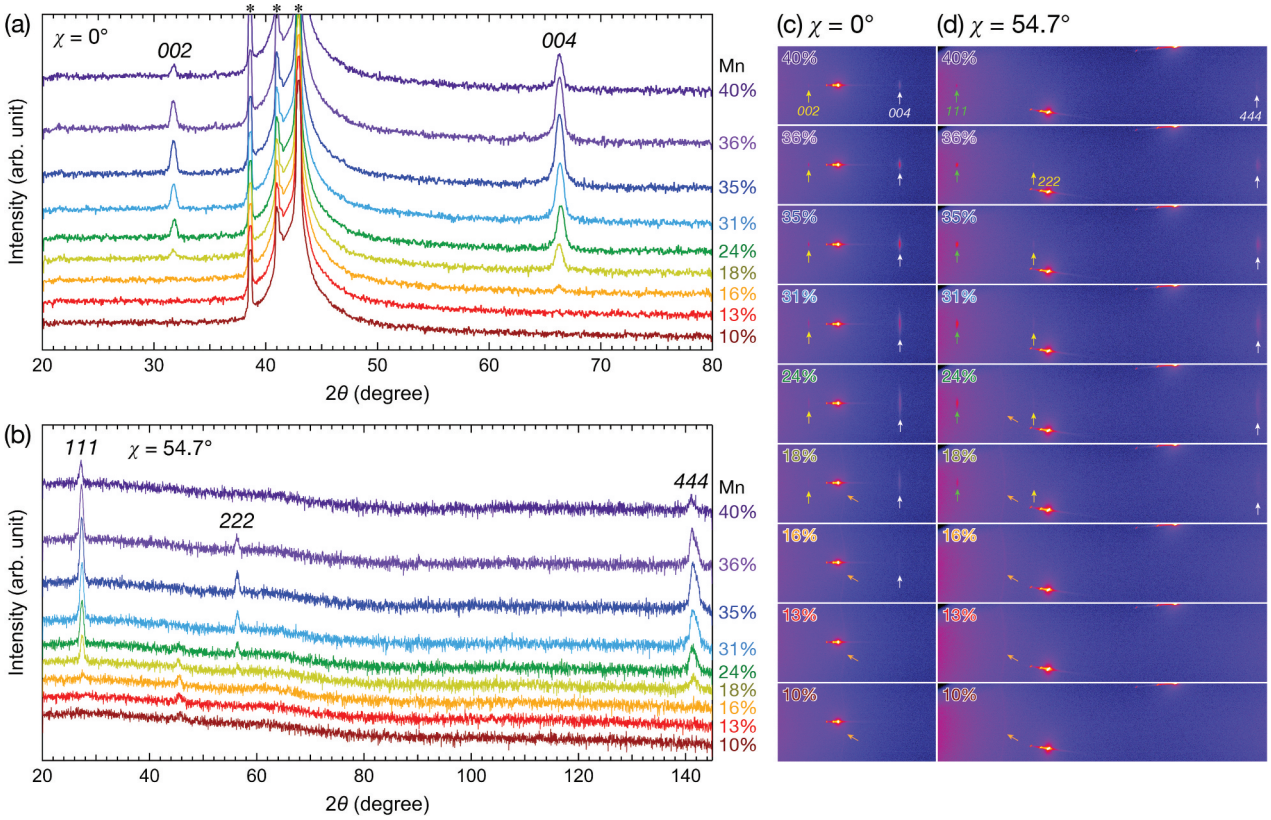

Figure 2. Compositional dependence on (a) out-of-plane ($\chi = 0°$) and (b) tilted-plane ($\chi = 54.7°$) one-dimensional (1D) X-ray diffraction (XRD) patterns of $Co_{75-x}Mn_xSi_{25}$ composition-spread film on MgO(100) substrate after post-annealing at 500°C. The diffraction peaks originated from MgO(100) substrate are indicated by the symbol *. Two-dimensional (2D) XRD images for $\chi = 0°$ and 54.7° are also shown in parts (c) and (d), respectively.

0° and 54.7° are also shown in Figure 2(c, d), respectively. For $x = 10\%$ and 13%, only ring-shaped diffraction peaks were observed at $2\theta \approx 45.4°$ for both $\chi = 0°$ and 54.7°, which might be originated from polycrystalline Co_2MnSi and/or silicides such as Co_2Si. Because the intensity of the ring-shaped peaks was very small, the effect on the electronic structures from HAXPES experiment and transport properties could be negligible. From $x = 16\%$, a weak fundamental peak from *004* was observed at $2\theta \approx 66.3°$ for $\chi = 0°$ along with the ring-shaped peaks. From $x = 18\%$, a spot-like superlattice diffraction peak originating from *002* at $2\theta \approx 31.8°$ began to be observed for $\chi = 0°$ along with a fundamental peak from *004*. For $\chi = 54.7°$, a spot-like superlattice *111* peak at $2\theta \approx 27.3°$ also began to be observed from $x = 18\%$ along with a fundamental *444* peak at $2\theta \approx 141.3°$. The appearance of the *111* peak indicates the $L2_1$-ordering of Co_2MnSi from $x = 18\%$. For a nearly stoichiometric composition of $x = 24\%$, the intensity for these peaks tended to be stronger and sharper than those observed for $x = 18\%$. In addition, a superlattice *222* peak was observed at $2\theta \approx 56.3°$ for $\chi = 54.7°$. The *004* peak was broad towards the titled direction in the 2D XRD image. The ring-shaped peaks were still observed for x up to 24%. With increasing x, the peak intensity of *111* increased, showed a maximum at $x = 31\%$, and decreased after further Mn composition. On the other hand, the broadening of the peaks towards the tilted direction in the 2D XRD images became smaller continuously until $x = 40\%$. The *222* peak disappeared at $x = 40\%$. The degrees of $L2_1$ and $B2$ order were estimated to be ≈ 1 for $x = 18$–40%, where *002* and *111* superlattice peaks were observable. As a result, the $L2_1$-ordering and (001)-oriented epitaxial growth of Co_2MnSi were confirmed for a relatively wide range of $x = 18$–40%. Because the *111* peak was observed for $\chi = 54.7°$, Co_2MnSi was grown with 45° in-plane rotation. Thus, the epitaxial relation can be denoted as MgO(001)[100] || Co_2MnSi (001)[110].

3.2. HAXPES spectra

The valence band HAXPES spectra of $Co_{75-x}Mn_xSi_{25}$ composition-spread films are shown in Figure 3(a). The magnified views of the spectra near E_F for $x = 10$–24% and 24–40% are shown in Figure 3(b,c), respectively. The spectra were normalized by the intensity at $E_B \approx 3$ eV for each spectrum, which is justified by the fact that the spin-integrated total DOS at $E - E_F \approx 3$ eV obtained from first-principles calculation show almost the same values in the curves between different Mn compositions, as will be shown later in Figure 5. From Figure 3, a systematic change in the spectra depending on the Mn composition was observed, which clearly shows the advantage of the usage of composition-

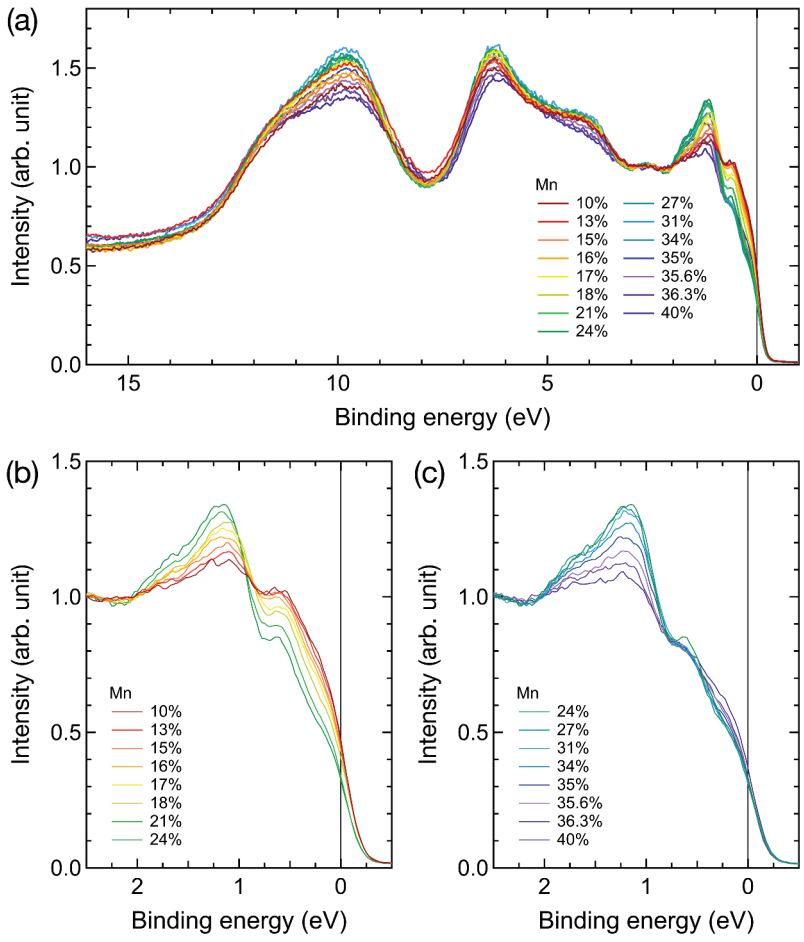

Figure 3. (a) Valence band hard X-ray photoelectron spectroscopy (HAXPES) spectra of $Co_{75-x}Mn_xSi_{25}$ composition-spread film. Magnified views near the Fermi level (E_F) of the spectra for (b) $x = 10$–24% and (c) $x = 24$–40%.

spread films in the photoemission spectroscopy experiment. The observed HAXPES spectra in this study agree well with those observed experimentally and with the simulated photoemission spectra of Co_2MnSi weighted by photoionization cross section in the previous reports [50,54–57,67–73]. From Figure 3(b), it can be seen that the intensity at E_F became smaller as x increased from the Mn-poorest composition of $x =$ 10% to the nearly stoichiometric composition of $x =$ 24%. From Figure 3(c), the intensity at E_F for the Mn-rich compositions changed slightly.

To make the change of intensity at E_F against the Mn composition more visible, the difference in intensity with respect to the spectrum for $x = 24\%$ is plotted in Figure 4(a). If the intensity of the spectrum is smaller than that for $x = 24\%$, the value becomes negative, and the largest negative value at E_F means the smallest intensity at E_F compared to the spectrum for

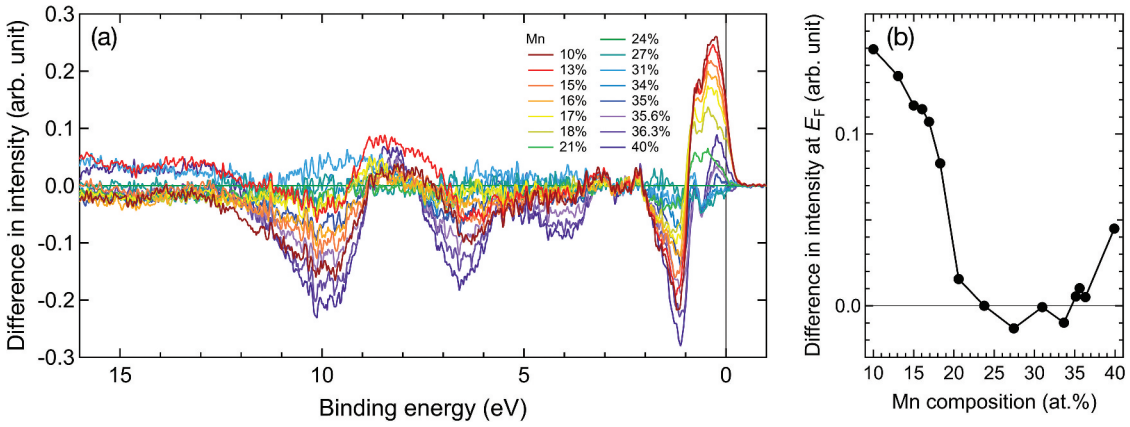

Figure 4. (a) Difference in intensity of valence band HAXPES spectra of $Co_{75-x}Mn_xSi_{25}$ composition-spread film with respective to the spectrum for $x = 24\%$. (b) Compositional dependence of difference in intensity at E_F.

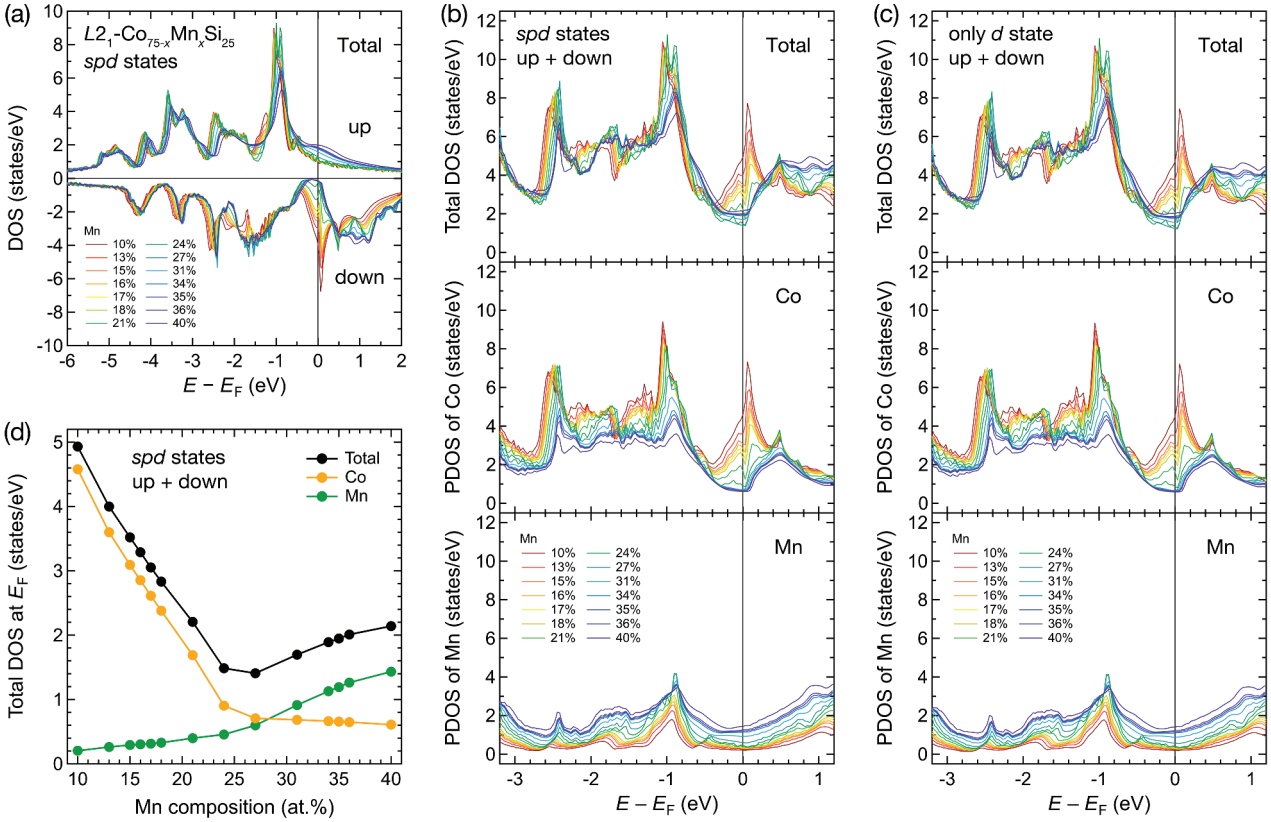

Figure 5. (a) Spin-resolved total density of states (DOS) of $L2_1$-ordered $Co_{75-x}Mn_xSi_{25}$ for *spd*-states of all atoms with different Mn compositions. Spin-integrated total DOS for all atoms and partial density of states (PDOS) for Co and Mn atoms for (b) *spd*-states and (c) only *d*-state. (d) Compositional dependence of spin-integrated total DOS for all atoms and PDOS for Co and Mn atoms for *spd*-states at E_F.

the nearly stoichiometric composition of $x = 24\%$. The compositional dependence of the difference in intensity at E_F is plotted in Figure 4(b). It is now clearly shown that the difference in intensity at E_F is the largest negative for $x = 27\%$, and it becomes larger as further increasing x up to the Mn-richest composition of $x = 40\%$. Thus, the intensity of the valence band HAXPES spectra at E_F was the smallest at E_F for a slightly Mn-rich composition of $x = 27\%$.

3.3. Density of states (DOS)

The spin-resolved total DOS of $L2_1$-ordered $Co_{75-x}Mn_xSi_{25}$ for *spd*-states of all atoms with different Mn compositions is shown in Figure 5(a). The formation of a half-metallic gap in the minority spin state was confirmed for $x = 27$–40%. When the Mn composition decreased from 24%, the in-gap states in the minority spin state around E_F began to increase and showed a maximum at $x = 10\%$ (*i.e.*, the Co-richest composition). On the other hand, for the majority spin state, the DOS around E_F showed almost the same for $x = 10$–27%. However, it began to increase as increasing x from 31% and showed a maximum broad peak at $x = 40\%$. These tendencies agree well with the calculation results in the previous reports [17,73].

Based on the spin-resolved DOS, spin-integrated total DOS for all atoms and PDOS for Co and Mn atoms for *spd*-states and only *d*-state are shown in Figure 5(b,c), respectively. The compositional dependence of the spin-integrated total DOS for all atoms and PDOS for Co and Mn atoms for *spd*-states at E_F is also plotted in Figure 5(d).

From Figure 5(d), the total DOS at E_F (black curve) was the smallest at $x = 27\%$. With decreasing x from 27%, the total DOS increased steeply and showed the largest at $x = 10\%$. With increasing x from 27%, the total DOS also increased but more gradually until $x = 40\%$. The PDOS of Co atoms at E_F (orange curve) began to increase steeply from $x = 24\%$ towards lower x (*i.e.*, higher Co composition) and showed a maximum at $x = 10\%$. On the other hand, the PDOS of Mn atoms at E_F (green curve) began to increase gradually from $x = 27\%$ and showed a maximum at $x = 40\%$. Based on these tendencies, the steep increase in the total DOS at E_F (black curve) for x lower than 27% can be originated from the steep increase in the PDOS for Co atoms at E_F (orange curve), while the gradual increase in the total DOS at E_F (black curve) for x higher than 27% can be originated from the gradual increase in the PDOS for Mn atoms at E_F (green curve).

By comparing the DOS for *spd*-states (Figure 5(b)) with the DOS for only *d*-state (Figure 5(c)), it is apparent that both the total DOS for all atoms and PDOS for Co and Mn atoms are dominated by the *d* state. Therefore, based on Figure 5(a,c), the steep increase in the PDOS for Co atoms at E_F (orange curve) for x lower than 27% should correspond to an increase in the in-gap states in the minority spin *d*-state, which leads to a steep reduction of spin polarization and destruction of half-metallicity. On the other hand, the gradual increase in the PDOS for Mn atoms at E_F (green curve) for x higher than 27% should correspond to an increase in the broad states of the majority spin *d*-state.

The large DOS in the majority spin *d*-state is not preferable for half-metallicity. For the other types of Heusler alloys such as Co_2CrAl [74,75] and Fe_2CrSi [76–78], they had received a certain attention because they were predicted to have large DOS in the majority spin state, which leads to a high spin polarization based on its definition. However, half-metallicity has not actually been confirmed in these materials. This would be because a large *d*-DOS in the majority spin state decreases the conductivity of *s* electrons in the majority spin state through *s*–*d* scattering process [79]. Based on the calculated DOS in Figure 5, the half-metallicity of $Co_{75-x}Mn_xSi_{25}$ tends to improve with increasing x due to a decrease in the DOS in the minority spin state and an increase in the *d*-DOS in the majority spin state. However, in terms of electrical transport, not only the spin polarization but also the scattering of *s* electrons by *d*-DOS at E_F should be considered [79]. Therefore, Heusler alloys possessing a half-metallic gap in the minority spin state and small *d*-DOS in the majority spin state at E_F can be considered as good half-metals.

As a result, the DOS calculation (Figure 5) shows that the total DOS at E_F was the smallest for $x = 27\%$, which is attributed to a half-metallic gap in the minority spin state and a small *d*-DOS in the majority spin state at E_F, indicating the best half-metallicity at this slightly Mn-rich composition. From the HAXPES results (Figure 4), the intensity of the valence band HAXPES spectra was the smallest for $x = 27\%$. Thus, the best half-metallicity among the Co_2MnSi composition-spread film can be detected by the spin-integrated HAXPES with the smallest intensity of the valence band HAXPES spectra at E_F.

3.4. AMR ratio

To further verify the half-metallicity of the Co_2MnSi composition-spread film in terms of transport properties, the AMR of the film was measured. The angular-dependent AMR of $Co_{75-x}Mn_xSi_{25}$ composition-spread film for the electric current direction along the [110] and [100] of Co_2MnSi is shown in Figure 6(a, b), respectively. The compositional dependence of the AMR ratio for *I*//[110] and [100] is plotted in Figure 6(c). All the curves showed two-fold symmetry. For *I*//[110], the AMR ratio was positive up to $x = 17\%$. The sign of the AMR ratio changed to negative at $x = 18\%$. The AMR ratio showed a negative maximum of −0.176% at $x = 27\%$, which was larger negative than that for the nearly stoichiometric composition of $x = 24\%$ of −0.168%. After further increasing x, the absolute value of the negative AMR ratio became smaller. For *I*//[100], the overall tendency for the compositional dependence of the AMR ratio was similar to that for *I*//[110]; the AMR ratio showed the negative maximum of −0.045% at $x = 27\%$, which was larger negative than that for $x = 24\%$ of −0.038%. The negative maximum value of the AMR ratio for *I*//[110] (−0.176% at $x = 27\%$) was larger than that for *I*//[100] (−0.045% at $x = 27\%$). The sign of the AMR ratio changed from positive to negative at $x = 24\%$ for *I*//[100], which was different from the case of *I*//[110] ($x = 18\%$). This means that the opposite sign of the AMR ratio between *I*//[110] and [100] was observed for $x = 18\%$ and 21% (Figure 6(c)).

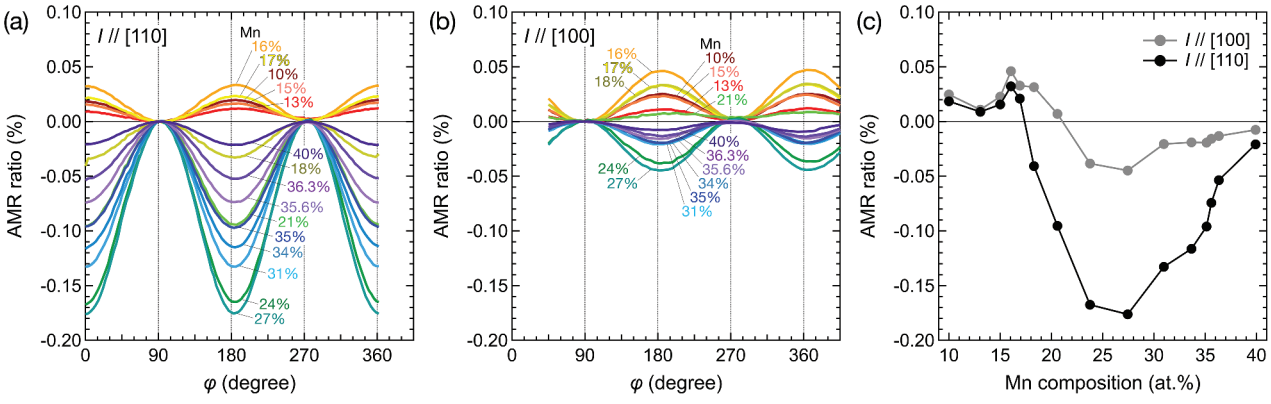

Figure 6. Angular-dependent AMR of $Co_{75-x}Mn_xSi_{25}$ composition-spread film for the electric current direction along the (a) *I*//[110] and (b) *I*//[100] of Co_2MnSi. (c) Compositional dependence of AMR ratio for *I*//[110] and [100].

The maximum negative AMR ratio of −0.176% for *I*//[110] at $x = 27\%$ in our $Co_{75-x}Mn_xSi_{25}$ composition-spread film was comparable to that observed in the previous studies of Co_2MnSi thin films [34,35,80–82]. In particular, the largest negative AMR ratio observed at the off-stoichiometric composition of $x = 27\%$ agrees with the previous study where the AMR ratio of Co_2MnSi thin films with slightly Mn-rich composition measured at 300 K was larger than that for the stoichiometric composition [82]. Conventional two-fold AMR curves were observed for all compositions and both current directions at 300 K in this study, which is also consistent with the previous reports [80,82].

Based on the previous experimental and theoretical studies [34–36,42,83–85], a larger negative AMR ratio in half-metallic Heusler alloys suggests a higher spin polarization, and thus, a smaller DOS at E_F in the minority spin states, leading to better half-metallicity. The largest negative AMR ratio was observed at $x = 27\%$ for both *I*//[110] and [100] (Figure 6(c)). Thus, the AMR results suggest that a slightly Mn-rich composition of $x = 27\%$ would possess the smallest DOS at E_F in the minority spin states, thus the best half-metallicity among the studied compositions, which supports the HAXPES and DOS calculation results. Because the half-metallicity of Co_2MnSi is very sensitive to Co_{Mn} anti-site [17–27], the excess Mn atoms would contribute to suppress the Co_{Mn} anti-site, leading to a better half-metallicity.

Recent theoretical analysis of AMR based on the electron scattering theory has suggested that when the dominant *s*–*d* scattering process is affected by the crystal field, the sign of the AMR ratio can sometimes be positive even for half-metallic materials depending on the electric current direction with respect to the crystal axis such as [110] and [100] [84]. In fact, the sign change of the AMR ratio depending on the current direction has been observed experimentally in Heusler alloys such as Co_2MnGa [86] and Mn_2VGa [87] for particular compositions. Hence, only measuring AMR for one particular current direction would not be sufficient to judge the half-metallicity of Heusler alloys. However, up until now, no systematic experimental study on the current direction dependence of AMR using systems with higher half-metallicity has been reported, which needs to be verified in the future. In our study based on the $Co_{75-x}Mn_xSi_{25}$ composition-spread film, combining the AMR results with the HAXPES and DOS calculation results, it is suggested that finding a composition showing a larger negative AMR ratio for both *I*// [110] and [100] may be a more reliable guideline for searching good half-metallicity of Heusler alloys, especially for Co_2MnSi thin films. The largest negative AMR ratio was observed for $x = 27\%$ for both *I*// [110] and [100] (Figure 6). Our HAXPES and DOS calculation results have indicated that this composition shows the best half-metallicity. Thus, measuring crystal-axis dependent AMR would provide more reliable insight into evaluating the half-metallicity of Heusler alloys.

Consequently, our results obtained from the HAXPES experiment, DOS calculation, and AMR measurement clearly indicate the best half-metallicity for the off-stoichiometric Mn composition of $x = 27\%$ in the $Co_{75-x}Mn_xSi_{25}$ composition-spread film. These results are consistent with each other. The change in the DOS at E_F, and thus the half-metallicity, was successfully detected by spin-integrated HAXPES of Co_2MnSi composition-spread films. Thus, high-throughput evaluation of the composition-dependent half-metallicity of Co_2MnSi Heusler alloys has been demonstrated by spin-integrated HAXPES using composition-spread films at NanoTerasu.

It is noteworthy that we were able to identify the composition exhibiting the best half-metallicity despite the use of *spin-integrated* HAXPES, which does not provide direct spin resolution. We would like to emphasize that this was possible only by combining spin-integrated HAXPES with composition-spread films, allowing us to systematically capture the changes in the electronic structures across different compositions in the composition-spread film. It would have been difficult to identify the composition with the best half-metallicity simply by analyzing the spectra of a few individual films with different compositions.

The high-throughput evaluation method would be suitable for obtaining a large amount of systematic data of composition-dependent electronic structures, deserving of machine learning and materials informatics. This would be beneficial for data-driven materials exploration of novel half-metals, leading to the development of efficient spintronic devices in the future.

4. Conclusion

We investigated the Mn-composition dependence on the half-metallicity of Co_2MnSi Heusler alloy using composition-spread films and spin-integrated HAXPES performed at BL09U of NanoTerasu. Our results obtained from the HAXPES experiment, DOS calculation, and AMR measurement consistently indicated the best half-metallicity for an off-stoichiometric slightly Mn-rich composition of $x = 27\%$ in the $Co_{75-x}Mn_xSi_{25}$ composition-spread film. The spin-integrated valence band HAXPES spectra exhibited the smallest photoemission intensity at E_F for $x = 27\%$. The DOS calculation showed that the total DOS at E_F was the smallest for $x = 27\%$, which is attributed to a half-metallic gap in the minority spin state and a small *d*-DOS in the majority spin state at E_F, indicating the

best half-metallicity at this composition. Thus, the best half-metallicity among the Co_2MnSi composition-spread film can be detected by the spin-integrated HAXPES with the smallest intensity of the valence band HAXPES spectra at E_F even without time-consuming spin resolution. From the AMR measurement, the largest negative AMR ratios of −0.176% and −0.045% were observed for $x = 27\%$ for both I//[110] and [100], respectively. Thus, it is suggested that finding a composition showing a larger negative AMR ratio for both current directions would provide a more reliable guideline for half-metallicity of Heusler alloys. Our high-throughput evaluation of the half-metallicity of Co_2MnSi Heusler alloys combining composition-spread films and spin-integrated HAXPES using high-brilliance synchrotron radiation will be beneficial for data-driven materials exploration for developing efficient spintronic devices in the future.

Acknowledgments

The authors thank S Kobari and R Kawahara from PhoSIC for the technical support with the HAXPES experiment. The authors thank N Kojima from NIMS for the technical support with the device fabrication and AMR measurement. The authors thank T Hiroto from NIMS for the technical support with the XRD measurement. The HAXPES experiment was performed under the approval of the coalition beamline of NanoTerasu. The x-ray diffraction measurement was performed on Surface and Bulk Analysis Unit in NIMS.

Disclosure statement

No potential conflict of interest was reported by the author(s).

Funding

This work was supported by the JST CREST (Grant No. JPMJCR21O1), the MEXT Program: Data Creation and Utilization-Type Material Research and Development Project (Digital Transformation Initiative Center for Magnetic Materials; Grant No. JPMXP1122715503), and the Innovative Science and Technology Initiative for Security (Grant No. JPJ004596), ATLA, Japan.

ORCID

Ryo Toyama http://orcid.org/0000-0002-7398-5803
Shunsuke Tsuda http://orcid.org/0000-0001-6209-8048
Yuma Iwasaki http://orcid.org/0000-0002-7117-277X
Thang Dinh Phan http://orcid.org/0000-0002-2446-0453
Susumu Yamamoto http://orcid.org/0000-0002-6116-7993
Hiroyuki Yamane http://orcid.org/0000-0002-8023-7918
Koichiro Yaji http://orcid.org/0000-0002-0721-1316
Yuya Sakuraba http://orcid.org/0000-0003-4618-9550

References

[1] Katsnelson MI, Irkhin VY, Chioncel L, et al. Half-metallic ferromagnets: from band structure to many-body effects. Rev Mod Phys. 2008;80(2):315–378. doi: 10.1103/RevModPhys.80.315
[2] Iwase T, Sakuraba Y, Bosu S, et al. Large interface spin-asymmetry and magnetoresistance in fully epitaxial Co_2MnSi/Ag/Co_2MnSi current-perpendicular-to-plane magnetoresistive devices. Appl Phys Express. 2009;2(6):063003. doi: 10.1143/APEX.2.063003
[3] Sakuraba Y, Hattori M, Oogane M, et al. Giant tunneling magnetoresistance in Co_2MnSi/Al-O/Co_2MnSi magnetic tunnel junctions. Appl Phys Lett. 2006;88(19):192508. doi: 10.1063/1.2202724
[4] Tsunegi S, Sakuraba Y, Oogane M, et al. Large tunnel magnetoresistance in magnetic tunnel junctions using a Co_2MnSi Heusler alloy electrode and a MgO barrier. Appl Phys Lett. 2008;93(11):112506. doi: 10.1063/1.2987516
[5] Hamaya K, Yamada M. Semiconductor spintronics with Co_2-Heusler compounds. MRS Bull. 2022;47(6):584–592. doi: 10.1557/s43577-022-00351-0
[6] Yamada S, Kato M, Ichikawa S, et al. Half-metallic heusler Alloy/GaN heterostructure for semiconductor spintronics devices. Adv Electron Mater. 2023;9(7):2300045. doi: 10.1002/aelm.202300045
[7] Elphick K, Frost W, Samiepour M, et al. Heusler alloys for spintronic devices: review on recent development and future perspectives. Sci Technol Adv Mater. 2021;22(1):235–271. doi: 10.1080/14686996.2020.1812364
[8] Chatterjee S, Chatterjee S, Giri S, et al. Transport properties of heusler compounds and alloys. J Phys: Condens Matter. 2022;34(1):013001. doi: 10.1088/1361-648X/ac268c
[9] Kämmerer S, Heitmann S, Meyners D, et al. Room-temperature preparation and magnetic behavior of Co_2MnSi thin films. J Appl Phys. 2003;93(10):7945–7947. doi: 10.1063/1.1556249
[10] Obaida M, Westerholt K, Zabel H. Magnetotransport properties of Cu_2MnAl, Co_2MnGe, and Co_2MnSi heusler alloy thin films: from nanocrystalline disordered state to long-range-ordered crystalline state. Phys Rev B. 2011;84(18):184416. doi: 10.1103/PhysRevB.84.184416
[11] Comtesse D, Geisler B, Entel P, et al. First-principles study of spin-dependent thermoelectric properties of half-metallic heusler thin films between platinum leads. Phys Rev B. 2014;89(9):094410. doi: 10.1103/PhysRevB.89.094410
[12] Guillemard C, Zhang W, Malinowski G, et al. Engineering $Co_2MnAl_xSi_{1-x}$ heusler compounds as a Model system to correlate spin polarization, intrinsic Gilbert Damping, and ultrafast demagnetization. Adv Mater. 2020;32(26):1908357. doi: 10.1002/adma.201908357
[13] Kudo K, Yamada S, Yafuso M, et al. Half-metallic nature of the low-temperature grown Co_2MnSi films on $SrTiO_3$. J Alloys Compd. 2021;854:155571. doi: 10.1016/j.jallcom.2020.155571
[14] Breidenbach AT, Yu H, Peterson TA, et al. Anomalous Nernst and Seebeck coefficients in epitaxial thin film $Co_2MnAl_xSi_{1-x}$ and Co_2FeAl. Phys Rev B. 2022;105(14):144405. doi: 10.1103/PhysRevB.105.144405

[15] Picozzi S, Continenza A, Freeman AJ. Co_2MnX (X = Si, Ge, Sn) heusler compounds: an ab initio study of their structural, electronic, and magnetic properties at zero and elevated pressure. Phys Rev B. 2002;66(9):094421. doi: 10.1103/PhysRevB.66.094421
[16] Webster PJ. Magnetic and chemical order in heusler alloys containing cobalt and manganese. J Phys Chem Solids. 1971;32(6):1221–1231. doi: 10.1016/S0022-3697(71)80180-4
[17] Picozzi S, Continenza A, Freeman AJ. Role of structural defects on the half-metallic character of Co_2MnGe and Co_2MnSi heusler alloys. Phys Rev B. 2004;69(9):094423. doi: 10.1103/PhysRevB.69.094423
[18] Miura Y, Nagao K, Shirai M. Atomic disorder effects on half-metallicity of the full-Heusler alloys $Co_2(Cr_{1-x}Fe_x)Al$: a first-principles study. Phys Rev B. 2004;69(14):144413. doi: 10.1103/PhysRevB.69.144413
[19] Galanakis I, Özdoğan K, Aktaş B, et al. Effect of doping and disorder on the half metallicity of full heusler alloys. Appl Phys Lett. 2006;89(4):042502. doi: 10.1063/1.2235913
[20] Ishikawa T, Liu HX, Taira T, et al. Influence of film composition in Co_2MnSi electrodes on tunnel magnetoresistance characteristics of Co_2MnSi/MgO/Co_2MnSi magnetic tunnel junctions. Appl Phys Lett. 2009;95(23):232512. doi: 10.1063/1.3272926
[21] Özdoğan K, Galanakis I. Effect of order on the half-metallic gap in Heusler compounds. J Appl Phys. 2011;110(7):076101. doi: 10.1063/1.3642990
[22] Liu HX, Honda Y, Taira T, et al. Giant tunneling magnetoresistance in epitaxial Co_2MnSi/MgO/Co_2MnSi magnetic tunnel junctions by half-metallicity of Co_2MnSi and coherent tunneling. Appl Phys Lett. 2012;101(13):132418. doi: 10.1063/1.4755773
[23] Li GF, Honda Y, Liu HX, et al. Effect of nonstoichiometry on the half-metallic character of Co_2MnSi investigated through saturation magnetization and tunneling magnetoresistance ratio. Phys Rev B. 2014;89(1):014428. doi: 10.1103/PhysRevB.89.014428
[24] Li S, Takahashi YK, Sakuraba Y, et al. Large enhancement of bulk spin polarization by suppressing Co_{Mn} anti-sites in $Co_2Mn(Ge_{0.75}Ga_{0.25})$ Heusler alloy thin film. Appl Phys Lett. 2016;108(12):122404. doi: 10.1063/1.4944719
[25] Moges K, Honda Y, Liu HX, et al. Enhanced half-metallicity of off-stoichiometric quaternary Heusler alloy Co_2(Mn,Fe)Si investigated through saturation magnetization and tunneling magnetoresistance. Phys Rev B. 2016;93(13):134403. doi: 10.1103/PhysRevB.93.134403
[26] Pradines B, Arras R, Abdallah I, et al. First-principles calculation of the effects of partial alloy disorder on the static and dynamic magnetic properties of Co_2MnSi. Phys Rev B. 2017;95(9):094425. doi: 10.1103/PhysRevB.95.094425
[27] Chen Z, Sakuraba Y, Miura Y, et al. Phase stability and half-metallic character of off-stoichiometric $Co_2FeGa_{0.5}Ge_{0.5}$Heusler alloys. J Appl Phys. 2022;132(18):183902. doi: 10.1063/5.0109802
[28] Takahashi S, Maekawa S. Spin injection and detection in magnetic nanostructures. Phys Rev B. 2003;67(5):052409. doi: 10.1103/PhysRevB.67.052409
[29] Takahashi YK, Kasai S, Hirayama S, et al. All-metallic lateral spin valves using $Co_2Fe(Ge_{0.5}Ga_{0.5})$ heusler alloy with a large spin signal. Appl Phys Lett. 2012;100(5):052405. doi: 10.1063/1.3681804
[30] Chen J, Sakuraba Y, Masuda K, et al. Enhancement of $L2_1$ order and spin-polarization in Co_2FeSi thin film by substitution of Fe with Ti. Appl Phys Lett. 2017;110(24):242401. doi: 10.1063/1.4985237
[31] Kushwaha VK, Sakuraba Y, Nakatani T, et al. High $L2_1$-atomic ordering and spin-polarization in Co_2MnZ (Z = Ge, Sn) heusler thin films with low-temperature annealing process. APL Mater. 2022;10(9):091119. doi: 10.1063/5.0117593
[32] Valet T, Fert A. Theory of the perpendicular magnetoresistance in magnetic multilayers. Phys Rev B. 1993;48(10):7099–7113. doi: 10.1103/PhysRevB.48.7099
[33] Nakatani T, Mihajlović G, Read JC, et al. High signal output in current-perpendicular-to-the-plane giant magnetoresistance sensors using In-zn-O-based spacer layers. Appl Phys Express. 2015;8(9):093003. doi: 10.7567/APEX.8.093003
[34] Yang FJ, Sakuraba Y, Kokado S, et al. Anisotropic magnetoresistance in Co_2(Fe,Mn)Si Heusler epitaxial films: a fingerprint of half-metallicity. Phys Rev B. 2012;86(2):020409(R. doi: 10.1103/PhysRevB.86.020409
[35] Sakuraba Y, Kokado S, Hirayama Y, et al. Quantitative analysis of anisotropic magnetoresistance in Co_2MnZ and Co_2FeZ epitaxial thin films: a facile way to investigate spin-polarization in half-metallic heusler compounds. Appl Phys Lett. 2014;104(17):172407. doi: 10.1063/1.4874851
[36] Kushwaha VK, Kokado S, Kasai S, et al. Prediction of half-metallic gap formation and fermi level position in Co-based Heusler alloy epitaxial thin films through anisotropic magnetoresistance effect. Phys Rev Mater. 2022;6(6):064411. doi: 10.1103/PhysRevMaterials.6.064411
[37] Iwasaki Y, Sawada R, Saitoh E, et al. Machine learning autonomous identification of magnetic alloys beyond the Slater-Pauling limit. Commun Mater. 2021;2(1):31. doi: 10.1038/s43246-021-00135-0
[38] Masuda H, Modak R, Seki T, et al. Large spin-hall effect in non-equilibrium binary copper alloys beyond the solubility limit. Commun Mater. 2020;1(1):75. doi: 10.1038/s43246-020-00076-0
[39] Toyama R, Kokado S, Masuda K, et al. Origin of negative anisotropic magnetoresistance effect in $Fe_{0.75}Co_{0.25}$ single-crystal thin films upon Ir addition. Phys Rev Mater. 2023;7(8):084401. doi: 10.1103/PhysRevMaterials.7.084401
[40] Toyama R, Zhou W, Sakuraba Y. Extrinsic contribution to the anomalous hall effect and Nernst effect in Fe_3Co single-crystal thin films by Ir doping. Phys Rev B. 2024;109(5):054415. doi: 10.1103/PhysRevB.109.054415
[41] Toyama R, Masuda K, Simalaotao K, et al. Large anomalous Nernst conductivity of $L1_0$-ordered CoPt in CoPt composition-spread thin films. J Phys D Appl Phys. 2024;57(40):405001. doi: 10.1088/1361-6463/ad460e
[42] Toyama R, Kushwaha VK, Sasaki TT, et al. Combinatorial optimization for high spin polarization in Heusler alloy composition-spread thin films by anisotropic magnetoresistance effect. APL Mater. 2023;11(10):101127. doi: 10.1063/5.0169124
[43] Wüstenberg JP, Fetzer R, Aeschlimann M, et al. Surface spin polarization of the nonstoichiometric Heusler alloy Co_2MnSi. Phys Rev B. 2012;85(6):064407. doi: 10.1103/PhysRevB.85.064407

[44] Jourdan M, Minár J, Braun J, et al. Direct observation of half-metallicity in the heusler compound Co_2MnSi. Nat Commun. 2014;5(1):3974. doi: 10.1038/ncomms4974
[45] Andrieu S, Neggache A, Hauet T, et al. Direct evidence for minority spin gap in the Co_2MnSi heusler compound. Phys Rev B. 2016;93(9):094417. doi: 10.1103/PhysRevB.93.094417
[46] Chernov S, Lidig C, Fedchenko O, et al. Band structure tuning of heusler compounds: spin- and momentum-resolved electronic structure analysis of compounds with different band filling. Phys Rev B. 2021;103(5):054407. doi: 10.1103/PhysRevB.103.054407
[47] Ueda S. Application of hard X-ray photoelectron spectroscopy to electronic structure measurements for various functional materials. J Electron Spectros Relat Phenom. 2013;190:235–241. doi: 10.1016/j.elspec.2013.01.009
[48] Goto K, Kumara LSR, Sakuraba Y, et al. Effects of the atomic order on the half-metallic electronic structure in the $Co_2Fe(Ga_{0.5}Ge_{0.5})$ heusler alloy thin film. Phys Rev Mater. 2020;4(11):114406. doi: 10.1103/PhysRevMaterials.4.114406
[49] Asai M, Miyazaki H, Watanabe K, et al. Hard X-Ray photoemission study of heusler-type $Fe_{2-x}Re_xVAl$ thermoelectric compounds. Phys Status Solidi B. 2022;259(9):2100567. doi: 10.1002/pssb.202100567
[50] Ueda S, Miura Y, Fujita Y, et al. Direct probing of temperature-independent bulk half-metallicity in Co_2MnSi by spin-resolved hard x-ray photoemission. Phys Rev B. 2022;106(7):075101. doi: 10.1103/PhysRevB.106.075101
[51] Ueda S, Sakuraba Y. Direct observation of spin-resolved valence band electronic states from a buried magnetic layer with hard X-ray photoemission. Sci Technol Adv Mater. 2021;22(1):317–325. doi: 10.1080/14686996.2021.1912576
[52] Schmitt M, Kirilmaz O, Chernov S, et al. Bulk spin polarization of magnetite from spin-resolved hard x-ray photoelectron spectroscopy. Phys Rev B. 2021;104(4):045129. doi: 10.1103/PhysRevB.104.045129
[53] Fetzer R, Ouardi S, Honda Y, et al. Spin-resolved low-energy and hard x-ray photoelectron spectroscopy of off-stoichiometric Co_2MnSi heusler thin films exhibiting a record TMR. J Phys D Appl Phys. 2015;48(16):164002. doi: 10.1088/0022-3727/48/16/164002
[54] Balke B, Fecher GH, Kandpal HC, et al. Properties of the quaternary half-metal-type heusler alloy $Co_2Mn_{1-x}Fe_xSi$. Phys Rev B. 2006;74(10):104405. doi: 10.1103/PhysRevB.74.104405
[55] Fecher GH, Balke B, Ouardi S, et al. High energy, high resolution photoelectron spectroscopy of $Co_2Mn_{1-x}Fe_xSi$. J Phys D Appl Phys. 2007;40(6):1576–1581. doi: 10.1088/0022-3727/40/6/S11
[56] Fecher GH, Balke B, Gloskowskii A, et al. Detection of the valence band in buried Co_2MnSi-MgO tunnel junctions by means of photoemission spectroscopy. Appl Phys Lett. 2008;92(19):193513. doi: 10.1063/1.2931089
[57] Modak R, Goto K, Ueda S, et al. Combinatorial tuning of electronic structure and thermoelectric properties in $Co_2MnAl_{1-x}Si_x$ Weyl semimetals. APL Mater. 2021;9(3):031105. doi: 10.1063/5.0041100
[58] Obara S, Ueshima K, Asaka T, et al. Commissioning of a compact multibend achromat lattice: a new 3 GeV synchrotron radiation facility. doi: 10.48550/arXiv.2407.08925
[59] Nishimori N, Watanabe T, Tanaka H. A highly brilliant compact 3 GeV light source project in Japan. Proc. 10th Int Particle Accelerator Conf (IPAC2019); 2019. p. 1478–1481. doi: 10.18429/JACoW-IPAC2019-TUPGW035
[60] Nishimori N. A new compact 3 GeV light source in Japan. In: Proc. 13th Int Particle Accelerator Conf (IPAC2022); 2022. p. 2402–2406. doi: 10.18429/JACoW-IPAC2022-THIXSP1
[61] Ueda S, Katsuya Y, Tanaka M, et al. Present status of the NIMS contract beamline BL15XU at SPring-8. AIP conf. Proc. 2010;1234:403–406. doi: 10.1063/1.3463225
[62] Okui M, Shimoguchi A, Yato N, et al. An experiment demonstrating the capability of a symmetrical layout type double crystal monochromator controlled using electronic cam technology. J Phys Conf Ser. 2022;2380(1):012054. doi: 10.1088/1742-6596/2380/1/012054
[63] Korringa J. On the calculation of the energy of a Bloch wave in a metal. Physica. 1947;13(6–7):392–400. doi: 10.1016/0031-8914(47)90013-X
[64] Kohn W, Rostoker N. Solution of the Schrödinger equation in periodic lattices with an application to metallic lithium. Phys Rev. 1954;94(5):1111–1120. doi: 10.1103/PhysRev.94.1111
[65] Akai H. Electronic structure of Ni–pd alloys calculated by the self-consistent KKR-CPA method. J Phys Soc Jpn. 1982;51(2):468–474. doi: 10.1143/JPSJ.51.468
[66] Akai KKR (machikaneyama). Ab-initio electronic-structure calculation code. http://kkr.issp.u-tokyo.ac.jp/
[67] Kandpal HC, Fecher GH, Felser C, et al. Correlation in the transition-metal-based heusler compounds Co_2MnSi and Co_2FeSi. Phys Rev B. 2006;73(9):094422. doi: 10.1103/PhysRevB.73.094422
[68] Kandpal HC, Fecher GH, Felser C. Calculated electronic and magnetic properties of the half-metallic, transition metal based heusler compounds. J Phys D Appl Phys. 2007;40(6):1507–1523. doi: 10.1088/0022-3727/40/6/S01
[69] Miyamoto K, Kimura A, Miura Y, et al. Absence of temperature dependence of the valence-band spectrum of Co_2MnSi. Phys Rev B. 2009;79(10):100405 (R. doi: 10.1103/PhysRevB.79.100405
[70] Chadov S, Fecher GH, Felser C, et al. Electron correlations in $Co_2Mn_{1-x}Fe_xSi$ Heusler compounds. J Phys D Appl Phys. 2009;42(8):084002. doi: 10.1088/0022-3727/42/8/084002
[71] Ouardi S, Balke B, Gloskovskii A, et al. Hard x-ray photoelectron spectroscopy of buried heusler compounds. J Phys D Appl Phys. 2009;42(8):084010. doi: 10.1088/0022-3727/42/8/084010
[72] Ouardi S, Gloskovskii A, Balke B, et al. Electronic properties of Co_2MnSi thin films studied by hard x-ray photoelectron spectroscopy. J Phys D Appl Phys. 2009;42(8):084011. doi: 10.1088/0022-3727/42/8/084011
[73] Kozina X, Karel J, Ouardi S, et al. Probing the electronic states of high-tmr off-stoichiometric Co_2MnSi thin films by hard x-ray photoelectron spectroscopy. Phys Rev B. 2014;89(12):125116. doi: 10.1103/PhysRevB.89.125116

[74] Galanakis I. Surface properties of the half- and full-heusler alloys. J Phys Condens Matter. 2002;14 (25):6329–6340. doi: 10.1088/0953-8984/14/25/303
[75] Ishida S, Kawakami S, Asano S. Theoretical predict of half-metals in Co-cr-fe-al alloys. Mater Trans. 2004;45(4):1065–1069. doi: 10.2320/matertrans.45.1065
[76] Mizutani S, Ishida S, Fujii S, et al. Half-metallic properties and stability of ferromagnetic state in the full-Heusler alloys $(Fe_xRu_{1-x})_2CrSi$ ($0 \leq x \leq 1$). Mater Trans. 2006;47(1):25–30. doi: 10.2320/matertrans.47.25
[77] Ishida S, Mizutani S, Fujii S, et al. Theoretical prediction of materials to preserve high spin polarization against chemical disorder. Mater Trans. 2006;47 (1):31–37. doi: 10.2320/matertrans.47.31
[78] Ishida S, Mizutani S, Fujii S, et al. Effect of chemical disorder on half-metallicity of Fe_2CrZ (Z = IIIb, IV, vb element). Mater Trans. 2006;47(3):464–470. doi: 10.2320/matertrans.47.464
[79] Kota Y, Takahashi T, Tsuchiura H, et al. Spin-polarized electronic structures and transport properties of Fe-co alloys. J Appl Phys. 2009;105(7):07B716. doi: 10.1063/1.3073955
[80] Oogane M, McFadden AP, Kota Y, et al. Fourfold symmetric anisotropic magnetoresistance in half-metallic Co_2MnSi heusler alloy thin films. Jpn J Appl Phys. 2018;57(6):063001. doi: 10.7567/JJAP.57.063001
[81] Oogane M, McFadden AP, Fukuda K, et al. Low magnetic damping and large negative anisotropic magnetoresistance in half-metallic $Co_{2-x}Mn_{1+x}Si$ heusler alloy films grown by molecular beam epitaxy. Appl Phys Lett. 2018;112(26):262407. doi: 10.1063/1.5030341
[82] Sato T, Kokado S, Kosaka S, et al. Large negative anisotropic magnetoresistance in Co_2MnGa Heusler alloy epitaxial thin films. Appl Phys Lett. 2018;113 (11):112407. doi: 10.1063/1.5047821
[83] Kokado S, Tsunoda M, Harigaya K, et al. Anisotropic magnetoresistance effects in Fe, Co, Ni, Fe_4N, and half-metallic ferromagnet: a systematic analysis. J Phys Soc Jpn. 2012;81(2):024705. doi: 10.1143/JPSJ.81.024705
[84] Kokado S, Tsunoda M. Theoretical study on anisotropic magnetoresistance effects of $I//[100]$, $I//[110]$, and $I//[001]$ for ferromagnets with a crystal field of tetragonal symmetry. J Phys Soc Jpn. 2019;88 (3):034706. doi: 10.7566/JPSJ.88.034706
[85] Kokado S, Sakuraba Y, Tsunoda M. Spin polarization ratios of resistivity and density of states estimated from anisotropic magnetoresistance ratio for nearly half-metallic ferromagnets. Jpn J Appl Phys. 2016;55 (10):108004. doi: 10.7567/JJAP.55.108004
[86] Sato T, Kokado S, Tsujikawa M, et al. Signs of anisotropic magnetoresistance in Co_2MnGa Heusler alloy epitaxial thin films based on current direction. Appl Phys Express. 2019;12(10):103005. doi: 10.7567/1882-0786/ab42b4
[87] Li ZH, Suto H, Barwal V, et al. Enhancing atomic ordering, magnetic and transport properties of Mn_2VGa heusler alloy thin films toward negatively spin-polarized charge injection. Acta Mater. 2024;276:120110. doi: 10.1016/j.actamat.2024.120110